Hathiram Guguloth, Santosh A / International Journal of Engineering Research and Applications (IJERA) ISSN: 2248-9622 www.ijera.com
Vol. 2, Issue 5, September- October 2012, pp.1874-1883

Simulation of DC/DC Boost Converter by using Three-Phase Indirect Matrix Converter

Hathiram Guguloth, Santosh A

Abstract

In this paper, a new circuit topology is presented, which is composed of an indirect matrix converter (IMC) and a dc/dc boost converter that connects to the neutral point of a motor. An indirect matrix converter (IMC) connected with two input power sources: a gasoline generator as the main ac power supply and batteries as the secondary power source. The IMC is small in size because of having a dc-link part without an electrolytic capacitor. The dc-link part is utilized by connection with a boost-up chopper with batteries as a secondary input power source. The proposed technique successfully further reduce the size of the converter by removing the boost reactor in the boost converter stage. The proposed converter is simulated and experimentally validated using a 750-W prototype and an induction motor driven with *V/f* control. The total harmonic distortion of the input and output currents are 4% and 3.7%, respectively, and the efficiency is 96%.

Index Terms—Boost-up chopper, leakage inductance, neutral point of a motor, three-phase ac/ac converter, zero-vector switching.

I.INTRODUCTION

Environmental responsibility has become a significant concern for communities so that the development of renewable power sources, such as wind turbines and low-carbon emission hybrid electric vehicles (HEVs) is progressing rapidly. One of the most common applied converters in hybrid systems is the ac/dc/ac converter because it has the ability of connecting to two different power sources. The generator mainly supplies constant power to the load and a battery is used as an alternate power source to drive an electric motor and also to absorb the power fluctuation during periods of high peak energy demand.

Fig. 1 shows a conventional ac/dc/ac power converter, which typically consists of a pulse width modulation (PWM) rectifier, a dc-link capacitor, and a PWM inverter, also known as a back to- back (BTB) system. The PWM rectifier is often used to reduce the harmonic currents in a generator and control the dc-link voltage. In order to obtain high performance under an adjustable speed drive system, a constant dc-link voltage is required in a BTB system because the voltage fluctuation of the dc-link part will cause an output voltage error. A typical method for reduction of the voltage fluctuation is to place a large electrolytic capacitor into the dc-link part as a filtering device between the rectifier and the inverter. However, a large electrolytic capacitor is bulky.

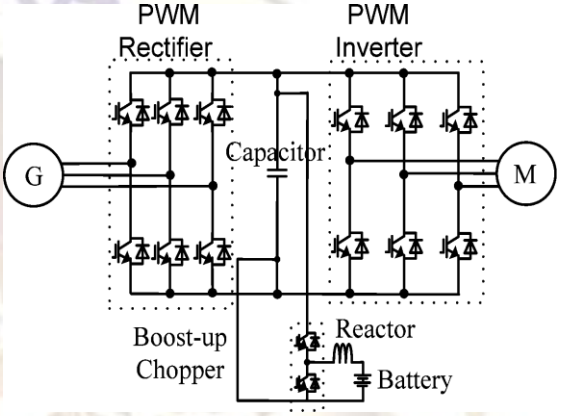

Fig. 1. Back-to-back converter.

Another approach is to reduce the capacity of the electrolytic capacitor by the application of a high-speed dc-voltage controller to the rectifier control. However, the control response is limited by the delay of the voltage detection and digital controller; therefore, the electrolytic capacitor is still required.

In addition, the capacitance is not reduced, since the dc-link capacitor is dominated by the capacitor current. As a result, a large amount of space is required for the capacitor installation in a practical device. In addition, electrolytic capacitors are not suitable for high-temperature applications, such as in HEVs. Overall, these disadvantages of the electrolytic capacitor affect the reliability of the converter.

For the secondary input power source, a boost converter that consists of a boost reactor and a switching leg [insulated gate bipolar transistor (IGBT)] is connected with batteries to the dc link part of the BTB system. Boost converter will control the battery current and the battery power will be used as a secondary power to drive the electric motor.

In this paper, a new circuit topology is presented, which is composed of an indirect matrix converter (IMC) and a dc/dc boost converter that connects to the neutral point of a motor. An IMC has high efficiency and is easily configured in comparison to matrix converters. In addition, this

converter does not require a dc-link electrolytic capacitor to filter the dc-ripple voltage. It uses a direct conversion technique where the frequency of the dc-link voltage contains a ripple with six times of the input frequency. However, the output voltage transfer ratio is limited by this direct conversion technique which is similar to the matrix converter, where output voltage = 0.866 of the input voltage.

Nevertheless, an appropriate control over the inverter is also proposed so that it is possible to connect a dc chopper to the neutral point of the motor and to operate as a dc/dc converter [14]. This dc/dc converter with a battery is performed as a secondary power source of the IMC to drive the electric motor. The proposed circuit utilizes the neutral point of a motor in the boost converter because the leakage inductance of the motor can be used as a reactor. Generally, the leakage inductance is around 10% of the rating impedance in an induction motor. For the proposed dc converter, around 3% of the reactor is enough to use as a boost reactor component. Please note that the synchronous reactance in a permanent motor is higher than the leakage inductance of an induction motor.

By removing the electrolytic capacitor and the boost-up reactor, the remaining part of the proposed circuit is constructed only of silicon components, namely, IGBTs and diodes. As a result, the proposed circuit is highly efficient and highly reliable. Simulation and experimental results clearly demonstrate that the circuit is capable of providing sinusoidal waveforms for the input and output, and high efficiency and a high power factor can be achieved.

II.PROPOSED CIRCUIT TOPOLOGY

Fig. 2 shows the proposed circuit configuration. The IMC can be simply divided into primary and secondary stages. The primary stage for the ac power source consists of 12 units of reverse-blocking IGBTs, also known as a current-source rectifier, where bidirectional power flow is possible in this circuit structure. A *LC* filter is required at the input of the primary stage to smooth the input current. The secondary stage for the motor consists of six IGBT units, which is similar to a standard voltage source inverter. The advantage of this converter over a BTB is that the primary side does not contain switching loss because zero-current switching can be applied. The switching timing of the primary side is during the zero-current period of the dc-link when the secondary stage output zero voltage. Therefore, high efficiency is achievable in this converter.

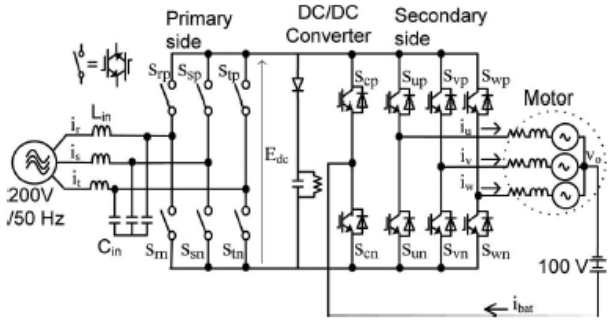

Fig.2. Proposed circuit topology.

The other reason to use the IMC is that the IMC has a dc-link part, which is different than the conventional matrix converter. The dc-link part is utilized by adding a boost converter to the IMC. The boost converter connects to the battery and the other terminal of the battery is then connected to the neutral point of the motor.

A snubber circuit is also included in the dc-link part to absorb the voltage overshoot from reactive elements in the circuit. It is used to prevent damage to the switching devices in the secondary side due to a sudden large voltage. It should be noted that the capacity of the snubber capacitor is smaller than the dc-link capacitor in a BTB system, because the ripple current of the dc-link part does not flow in the snubber capacitor.

The chopper circuit is connected in the dc link and batteries are connected to the neutral point of the motor. The leakage inductance of the motor is used as a boost-up reactor in the proposed circuit. As a result, the proposed converter does not require bulky passive components.

III.CONTROL STRATEGY

Fig. 3(a) shows a control block diagram of the proposed circuit. The primary side, the dc chopper, and the secondary side are individually controlled by their own commands. A carrier comparison method is used as the PWM modulation, according to the control strategy.

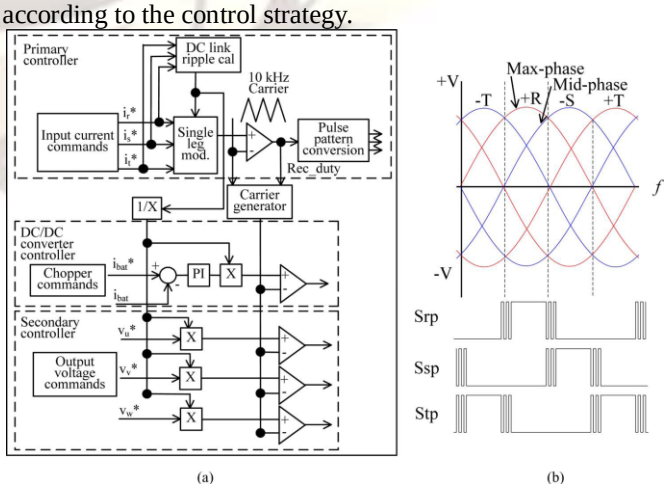

Fig. 3 (a) Control block diagram. (b) Primary-side-switching pattern.

The relationship between the output and input voltages is obtained by (1). The secondary side operates as a four-phase voltage-source inverter by addition of the dc chopper as the fourth leg

$$\begin{bmatrix} v_u \\ v_v \\ v_w \\ v_{\text{bat}} \end{bmatrix} = \begin{bmatrix} s_{up} & s_{un} \\ s_{vp} & s_{vn} \\ s_{wp} & s_{wn} \\ s_{cp} & s_{cn} \end{bmatrix} \begin{bmatrix} s_{rp} & s_{sp} & s_{tp} \\ s_{rn} & s_{sn} & s_{tn} \end{bmatrix} \begin{bmatrix} v_r \\ v_s \\ v_t \end{bmatrix} \quad (1)$$

where s_{xy} represents the switching function of the switches. When s_{xy} is turned ON, $s_{xy} = 1$, and when s_{xy} is turned OFF, $s_{xy} = 0$.

A. Primary-Side Control

The primary-side controller is designed with a current-type PWM rectifier command. It uses a pulse-pattern conversion to convert the PWM pulses of the voltage source type into the PWM pulse of the current source type by a simple logic selector. It uses a single-leg modulation where the switching period can be reduced from $2\pi/3$ to $\pi/3$, where the $2\pi/3$ is the switching period of the conventional two-phase modulation. That is, the leg with the maximum input phase voltage will always be turned ON, and the other two legs will be always turned OFF, as shown in Fig. 3(b). When the maximum input phase voltage is changing, (for example, from $+R$-phase to $-S$-phase), the related max phase voltage leg and the mid phase voltage leg will be switched at zero current until the relevant switch that contains the mid phase voltage becomes the maximum input phase voltage. From this direct conversion technique, a dc-link voltage that contains a ripple with six times of the input frequency will be formed.

B. Secondary-Side Control

A conventional controller method for a voltage-source-type inverter is applied to the dc chopper and the inverter with a lean controlled carrier modulation. The carrier modulation forms a new carrier, where the peak position of the triangular carrier is controlled by the duty ratio of the rectifier-side pulse. This rectifier pulse is used to control the switching timing of the primary stage and the zero-vector of the secondary stage. From the control, zero-current switching is achieved in the primary stage, where the dc-link current becomes zero at the peak of every carrier. This new carrier is then used in the secondary side and the dc chopper side as a normal PWM comparison method, also referred to as an inverter carrier.

The boost converter is not a stand-alone circuit in the proposed circuit. Operation is strongly dependent on the secondary side of the IMC. Zero-vector outputs on the secondary side are the key factor to link the boost converter to the IMC. The zero vector controls the amplitude of the output voltage. There are two functions of the zero-vector output to the secondary side. The first is to implement zero-current switching on the primary side so that the switching losses do not occur at the primary side. The second function involves operation of the boost converter, which will be described in a later chapter.

Fig. 4 shows an example of the relationship between the normal carrier applied to the primary side and the new inverter carrier applied to the secondary side. The inverter commands are given by the voltage controller as described in Chapter IV. It is noted that the dc chopper is controlled as the fourth leg of the inverter so that the dc chopper command is compared by the same carrier with the inverter voltage commands. There are two methods to generate an inverter carrier; Fig. 4(a) represents the symmetrical type, which has approximately double the switching frequency of the rectifier switching frequency, and Fig. 4(b) shows the asymmetrical type, which has the same switching frequency as the rectifier switching frequency.

In Fig. 4(a), the bottom peak position of the triangular carrier is controlled by the duty ratio of the rectifier pulse, as shown in the upper part of the figure. The chopper commands, along with the inverter output voltage commands, are compared with this new inverter carrier to obtain the desired switching patterns. The zero-vector periods are shown in the lower part of Fig. 4(a). The switching pulses of the secondary side attain the zero vectors for every carrier cycle. The primary side arms switch at every zero-vector period.

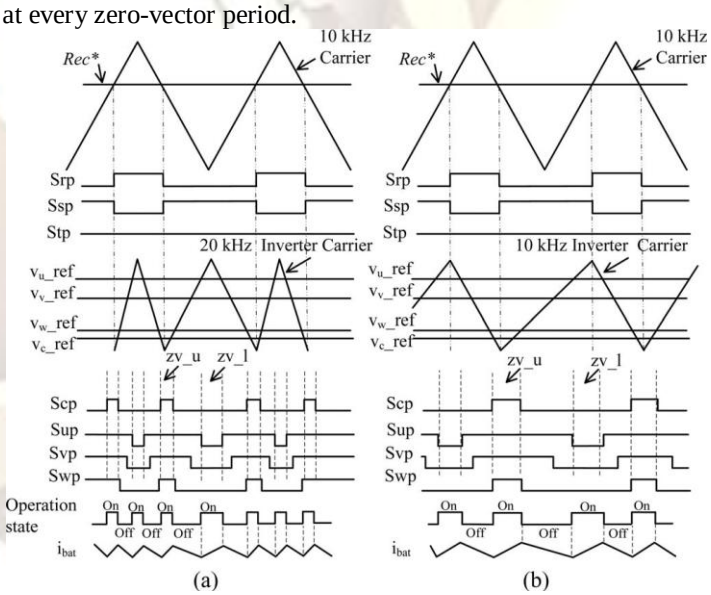

Fig. 4. Relationship between the zero vectors and boost converter operation.
(a) Symmetrical inverter carrier. (b) Asymmetrical inverter carrier.

In Fig. 4, zv_*u* and zv_*l* represent the zero-vector periods of the inverter, where zv $u = S_{up} = S_{vp} = S_{wp} = 1$ (upper arm zero vector) and zv_$l = S_{up} = S_{vp} = S_{wp} = 0$[lower arm zero vector ($S_{un} = S_{vn} = S_{wn} = 1$)]. The upper arm of the chopper (S_{cp}) switches ON

at every zero-vector period of zv_*u*. On the other hand, the lower arm of the chopper (*Scn*) will switch ON at every zero-vector periods of zv_*l*. During these zero-vector periods, the boost converter is operated in the ON-state, and the battery current through the leakage inductance of the motor increases. During the nonzero-vector periods, also known as the OFF-state operation, the battery current is released into the capacitor in the *LC* filter at the power source. The operation state in the figure is referred to the boost converter operation.

When the switching frequency of the rectifier is 10 kHz, the control method applied in Fig. 4(a) generates a new symmetrical carrier that has a frequency of approximately 20 kHz. This is approximately twice the primary-side switching frequency. Alternatively, according to Fig. 4(b), an inverter carrier can be formed based on the duty of the rectifier command, which is asymmetrical with a frequency of 10 kHz.

By comparing the symmetrical and asymmetrical inverter carriers in Fig. 4, it should be noted that the zero-current switching in the rectifier is not affected by the inverter carrier because both carriers are formed following the rectifier duty. Since every carrier time is longer in the asymmetrical inverter carrier, the sequence of the zero-vector periods becomes slower; therefore, the boost converter will achieve better efficiency, but the current ripple in the battery will be increased. Further, the asymmetrical method can achieve better total harmonic distortion (THD) values for the output because the dead time effect is smaller due to the lower switching frequency.

The other disadvantage of the asymmetrical inverter carrier is the detection of the load current. Usually, the average value of the load current appears at the peak of the symmetrical inverter carrier so that it can be easily detected using the symmetrical inverter carrier. However, for the asymmetrical carrier, the average current point does not agree with the peak of the asymmetrical carrier; therefore, in order to detect the average current, a low pass filter is required. Consequently, control performance will be decreased.

IV.UTILIZATION OF THE NEUTRAL POINT OF THE MOTOR

The voltage commands of the secondary stage are decided by the battery current command and the output voltage commands for the three-phase load. A three-phase inverter has eight output voltage space vectors, including two zero vectors. The importance of the zero vectors explains the behavior of the boost converter along with the neutral point of the motor. The boost converter will operate at every zero vector of the secondary side of the converter. On the other hand, the output voltage for the three-phase load is controlled by other voltage vectors.

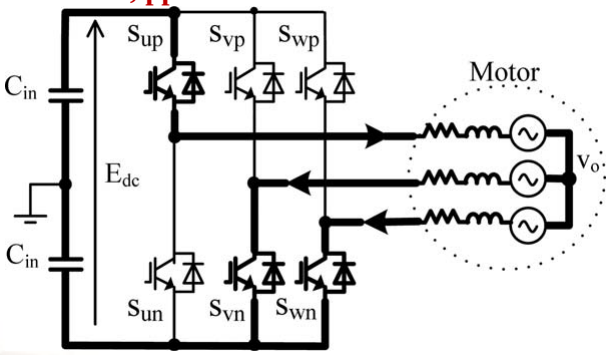

Fig. 5. Secondary-side current flow diagram (normal operation).

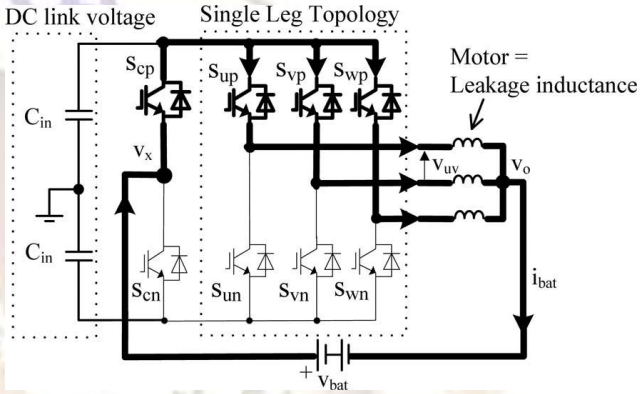

Fig. 6. Zero-phase-sequence equivalent circuit.

Fig. 5 illustrates the output current-flow diagram of the secondary side under the normal operation and Fig. 6 shows the zero-phase-sequence equivalent circuit, where the battery is operating at discharge mode. In Fig. 5, the secondary side functions as a conventional three-phase inverter with a motor; it controls the motor speed and torque. Zero-phase sequence is happening at every zero-vector periods of the secondary side. The current at the neutral point of the motor is zero and a positive or negative battery current can be controlled, as shown in Fig. 6. Note that the polarity of the battery voltage can be connected in facing the neutral point of the motor or in a reverse way. C_{in} represents the capacitors from the *LC* filter; since two switches in the primary side will always be turned ON, the capacitors C_{in} can be considered in the dc-link voltage. On the other hand, for the zero-phase sequence, the motor line voltage can be considered as zero so that the motor can be considered as a leakage inductance. In addition, the secondary side of the converter can be considered as a single-leg topology. The battery current first goes into the secondary side and flows out through the neutral line and charges or discharges the battery. The battery current can be controlled by the proportional–integral (PI) controller.

The zero vectors are two particular vectors that generate zero line voltage to the motor. The neutral-point voltage *v*0 of the motor, based on the

neutral point of the dc-link part, is obtained by the following equation:

$$\begin{cases} v_0 = \dfrac{E_{\mathrm{dc}}}{2}, & \text{When all upper arms are ON} \\ v_0 = \dfrac{-E_{\mathrm{dc}}}{2}, & \text{When all lower arms are ON} \end{cases} \quad (2)$$

where E_{dc} is the dc-link voltage and $v0$ is the voltage of the neutral point of the motor, based on the neutral point of the dc-link part.

A high dc-link voltage is mandatory in order to control the zero vectors; therefore, the relationship between the dc-link voltage (E_{dc}), the inverter line voltage (v_{inv}), and the battery voltage (V_{bat}) will be discussed. The inverter output voltage, v_u , v_v , and v_w , with respect to the neutral point voltage of the dc link, is expressed as

$$\begin{cases} v_u = a\dfrac{E_{\mathrm{dc}}}{2}\sin\omega t + v_0 \\ v_v = a\dfrac{E_{\mathrm{dc}}}{2}\sin\left(\omega t - \dfrac{2\pi}{3}\right) + v_0 \\ v_w = a\dfrac{E_{\mathrm{dc}}}{2}\sin\left(\omega t - \dfrac{4\pi}{3}\right) + v_0 \end{cases} . \quad (3)$$

where a is the modulation index of the motor phase voltage, $0 < a < 1$, $v0$ is the neutral point voltage of the motor (during zero phase sequence), and ω is the inverter output angular frequency. The inverter line voltage is then given by (u–v phase)

$$v_{uv} = a\frac{\sqrt{3}}{2}E_{\mathrm{dc}}\sin\left(\omega t + \frac{\pi}{6}\right). \quad (4)$$

Equation (5) shows the relationship for an inverter to obtain the maximum output line voltage Vinv (rms) under the maximum reference magnitude of a three-phase modulation

$$E_{\mathrm{dc}} \geq 2\frac{\sqrt{2}}{\sqrt{3}}V_{\mathrm{inv}}. \quad (5)$$

The maximum line voltage between the inverter leg and chopper leg can be obtained as (rms)

$$v_{ux} = \frac{\sqrt{2}}{\sqrt{3}}V_{\mathrm{inv}} + V_{\mathrm{bat}}. \quad (6)$$

Since vux must be smaller than Edc, the inverter voltage and battery voltage are constrained by the following equation:\

$$E_{\mathrm{dc}} > \frac{\sqrt{2}}{\sqrt{3}}V_{\mathrm{inv}} + V_{\mathrm{bat}}. \quad (7)$$

TABLE I
SIMULATION PARAMETERS

As a result, the dc-link voltage of the proposed circuit must satisfy both requirements as shown by the following equation, which can be referring to Fig. 6:

$$E_{\mathrm{dc}} \geq \begin{cases} 2\dfrac{\sqrt{2}}{\sqrt{3}}V_{\mathrm{inv}}, & \text{When } \dfrac{\sqrt{2}V_{\mathrm{inv}}}{\sqrt{3}} \geq V_{\mathrm{bat}} \\ \dfrac{\sqrt{2}}{\sqrt{3}}V_{\mathrm{inv}} + V_{\mathrm{bat}}, & \text{When } \dfrac{\sqrt{2}V_{\mathrm{inv}}}{\sqrt{3}} < V_{\mathrm{bat}}. \end{cases} \quad (8)$$

Note that in (8), the V_{bat} can always be neutralized with half of the E_{dc} under the two conditions. That is, V_{bat} must be always smaller than half of the E_{dc}, since the E_{dc} is always known as the 0.866 of the input phase voltage, as shown in the following equation:

$$\frac{\sqrt{2}}{2}V_{\mathrm{in}}0.866 > V_{\mathrm{bat}}. \quad (9)$$

Furthermore, a new expression of the secondary-side current is given as follows, assuming that the leakage impedance is even during the zero-phase-sequence equivalent circuit

$$\begin{cases} i_u = i_a + \dfrac{i_{\mathrm{bat}}}{3} \\ i_v = i_b + \dfrac{i_{\mathrm{bat}}}{3} \\ i_w = i_c + \dfrac{i_{\mathrm{bat}}}{3} \end{cases} \quad (10)$$

where i_u , i_v , and i_w are the inverter currents, i_a , i_b , and i_c are the positive-phase-inverter current, and i_{bat} is the battery current.

V. SIMULATION RESULTS

Table I shows the simulation parameters for both results. The proposed circuit was simulated under two conditions of battery discharge and charge by using a circuit simulator (PSIM, *Powersim Technologies Inc.*). An automatic current regulator (ACR) controller controls the battery current to a desired positive or negative value. An ideal battery current $i$bat is purposely adjusted at a specific time of 38 ms to confirm the proposed circuit performance. The motor model, which consists of three sets of voltage sources as back-electromotive forces and leakage inductances, is used in the simulation. The asymmetrical inverter carrier was used in the simulation.

Input voltage	200 V	DC source	100 V
Input frequency	50 Hz	Output voltage	173 V
Carrier frequency	10 kHz	Output frequency	35 Hz
Inverter frequency	10 kHz	Leakage inductance	5 mH

Fig. 7 shows the battery discharge mode, with the battery current controlled from 0.5 to 2 A. The two waveforms show the input power supply voltages *vr* , *vs* , and *vt* , the input currents *ir* , *is* , and *it* , and the output line voltages (*vuv*(LPF) , *vvw*(LPF) , and *vwu*(LPF)) through a low-pass filter, which has a cutoff frequency of 1 kHz, to observe the low-frequency components, the output currents *iu* , *iv* , and *iw* , and the battery current *i*bat . The results show that the THD of both the input and output currents are less than 4%. It should be noted that at 20 ms, the input current magnitude decreases due to the increment of *i*bat , which indicates that the increase of the battery power leads to a decrease in generator power.

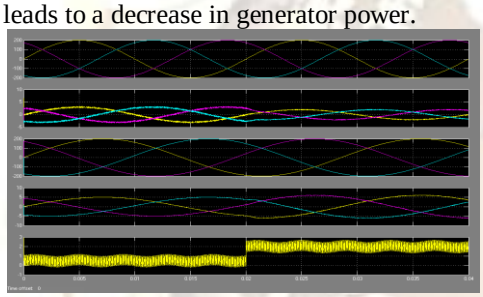

Fig. 7. Simulation results (battery = discharge mode).

On the other hand, Fig. 8 shows the ACR controlling the battery current from 0.5 to −2 A. The battery is charged from a generator under this condition. The results also showed that when in the charging mode, both the input and output currents have good sinusoidal waveforms. At 20 ms, as the *i*bat decreases, the input current is forced to increase, because higher power is required to charge the battery. These two waveforms provide evidence of good power management between the generator and the battery.

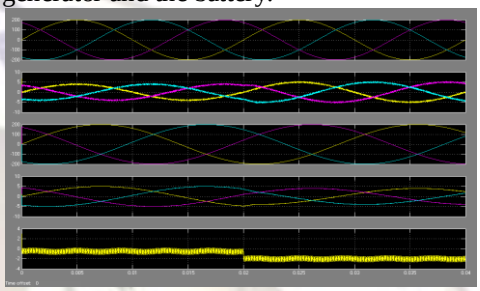

Fig. 8. Simulation results (battery = charge mode).

VI. EXPERIMENTAL RESULTS

A 750-W prototype was built and tested using two operation modes, the same as those described in the simulation section. Mode I is battery discharge under motoring operation, and Mode II is battery charge under motoring operation. Both conditions were verified using the parameters shown in Table II. The controller used the asymmetrical format to generate the 10-kHz inverter carrier. Table III shows the specification data for the motor. Note that this is conventional motor with no particular settings required for the neutral-point connection.

TABLE II
EXPERIMENTAL PARAMETERS

Input voltage	200 V	Inductor	1.7 mH
Input frequency	50 Hz	Capacitor	2.5 μF
Carrier frequency	10 kHz	DC source	100 V
Output frequency	30 Hz	LC Filter Cut-off frequency	2.4 kHz

TABLE III
MOTOR PARAMETERS (FUJI: MLH6085M)

Motor Power	750 W	Rated current	3.6 A
Poles	4/ 50 Hz	Rated voltage	200 V
RPM	1420	Leakage inductance	4.42 mH

TABLE IV
DEVICE PARAMETERS

	Primary side	Secondary side	Chopper
Devices model	1MBH30D-060 (Fuji Electric)	2MBI50N-060 (Fuji Electric)	2MBI50N-060 (Fuji Electric)
Collector-Emitter voltage	600 V	600 V	600 V
Gate-Emitter voltage	±20 V	±20 V	±20 V
Collector current	30 A	50 A	50 A
Turn-on time (Typ.)	0.16 μs	0.6 μs	0.6 μs
Turn-off time (Typ.)	0.30 μs	0.6 μs	0.6 μs
Reverse recovery time	300 ns	300 ns	300 ns

A. Fundamental Operations

Figs. 9 and 10 show the Mode I and Mode II operations, respectively. In Fig. 9, the dc power supply is set to 100 V and the battery current is controlled to 2 A. Similarly, in Fig. 10, the battery current is controlled to −2 A. Good sinusoidal waveforms were achieved for the input and output current of both operation modes.

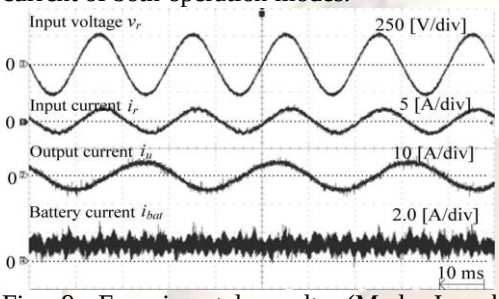

Fig. 9. Experimental results (Mode I = battery discharge).

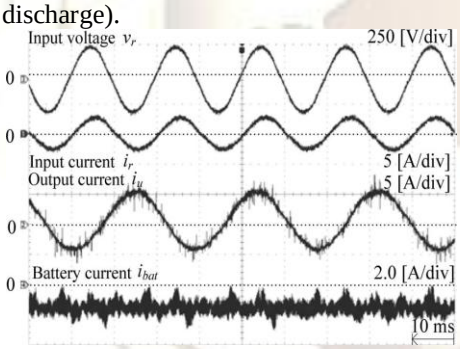

Fig. 10. Experimental results (Mode II = battery charge).

Fig. 11 shows the input power factor of the discharge and charge modes. Both modes achieved input power factors of more than 98%, which can be considered as a unity power factor. The input power factor decreases during the discharge mode because the input current becomes smaller in comparison with the charge mode.

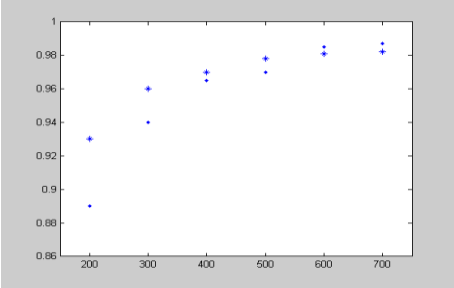

Fig. 11. Input power factor.

Fig. 12 shows the input current THD and the output current THD for both modes. The input current THD obtained during the charge mode is 3.6%, and that during the discharge mode is 4.0%. The lowest output current THD obtained during the charge mode is 3.0% and that during the discharge mode is 3.7%.

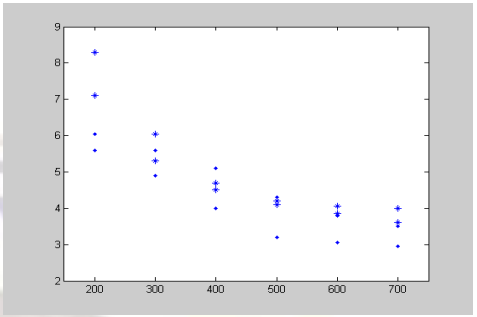

Fig. 12. Input and output current THD values.

Fig. 13 shows the picture of the prototype. All switching units are mounted on top of a heat sink. The top of the picture shows the primary-side-switching units.GateDrive Unit (GDU) boards are placed on top of the primary-side-switching units. The picture also shows that the switching units for the secondary side and the boost converter are based on a single-module IGBT unit.

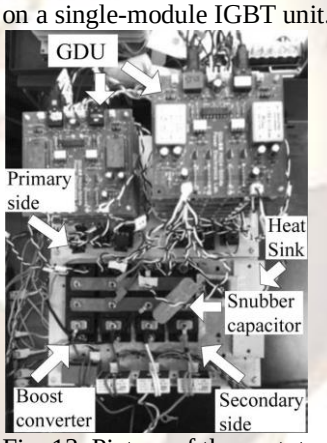

Fig. 13. Picture of the prototype.

B. Motor Performance Analysis

Fig. 14 demonstrates motor-related experimental results in order to confirm the motor performance for the proposed circuit. This figure shows the torque impact characteristic of the tested motor. The output frequency is 30 Hz, and the step increase of torque is 100%. The battery power is set at 200 W, and the input power is closely to 50 W when the torque is 0%. The input current *ir* shows a bad quality of waveform due to the low input power, since battery power is supplying the induction motor. When the torque increases to 100%, the battery power maintains at 200 W, subsequently the input power provides the additional required power to keep the motor speed. The rpm waveform demonstrates a good control of speed and the output current shows a corresponding sinusoidal waveform.

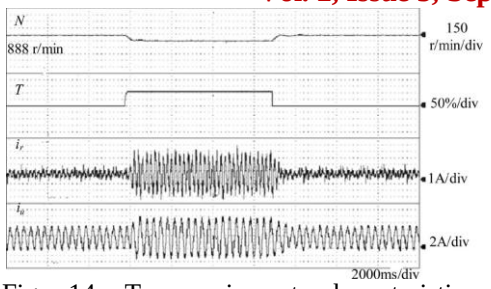

Fig. 14. Torque impact characteristic of the proposed circuit.

C. Efficiency and Loss Analysis

The loss analysis of the proposed circuit is now discussed, which is carried out using a circuit simulator (PSIM, *Powersim Technologies Inc.*) and dynamic link library (DLL) files [18]. The analysis was conducted for two categories, by application of the symmetrical and asymmetrical inverter carriers. Figs. 15– 18 show the loss analysis results simulated under the parameters as shown in Tables I, and IV shows the devices parameter. Note that in the loss analysis, the primary side is assumed to use reverse blocking IGBT (RB-IGBT). The output power is 750 W and the input power ratio is 9:1 in Figs. 15 and 16. The input power ratio is referring between the generator power and battery power, respectively. A ratio of 9:1 means that the total input power supplied from the generator power is 90% and the remaining 10% is supplied from the battery power.

Fig. 15 shows the details of the switching losses when the symmetrical inverter carrier is applied. Zero-current switching is implemented on the primary side, and therefore, conduction loss occurs only in that side. The total loss for the discharge mode is approximately 27 W, and that for the charge mode is approximately 29 W. The analysis verifies that the converter can achieve an efficiency of 96.4%.Aconventional back-to-back converter may achieve an efficiency of approximately 93% [19].

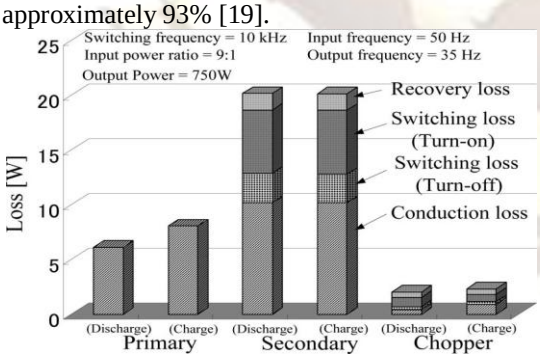

Fig. 15. Loss analysis—Switching device losses (symmetric method).

Two reasons are found for the higher losses in the secondary side. The first is that the switching frequency in the secondary side is 20 kHz when using the symmetric method, as discussed in Section III. The second reason is that the inverter current contains the battery current during the zero phase sequence. The higher switching frequency and larger battery current resulted in increased losses.

Fig. 16 shows the results of the asymmetric inverter carrier loss analysis, which was simulated under the same conditions as those for Fig. 15. The loss in the secondary side decreases approximately 20% and the loss in the chopper decreases by approximately 25%. The total loss for the discharge mode is 23 W and that for the charge mode is 25 W. An efficiency of 96.9% can be achieved, which is an improvement of approximately 0.5%.

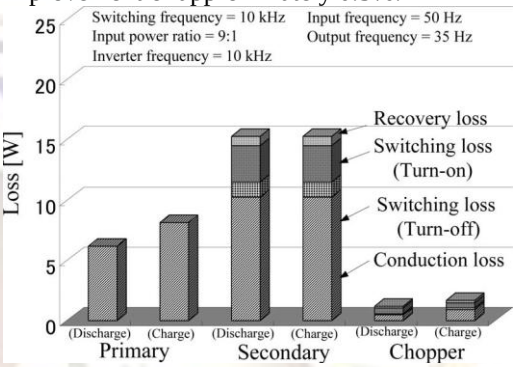

Fig. 16. Loss analysis–Switching device losses (asymmetric method).

Furthermore, in comparison the proposed circuit with the typical IMC, provided the energy flow is from ac to ac only, the efficiency is almost equivalent for the proposed circuit. However, for dc to ac, the motor loss will affect the efficiency, where a special type of motor with a connectable neutral point is required in order to reduce the copper loss in the motor.

Figs. 17 and 18 show the calculations of loss analysis by powering with various input power ratios from 10:0 to 1:9, which represent the ratio of the generator power to battery power. In this case, the losses in chopper gradually increase as the battery power is going larger. The losses in primary side decrease accordingly to the input power.

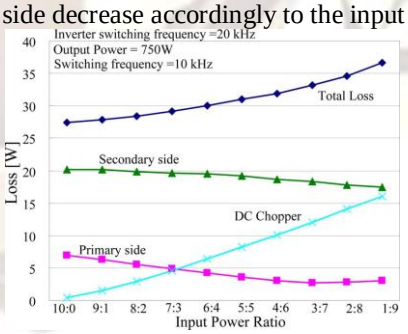

Fig. 17. Loss analysis—Changes in input ratio (symmetric method).

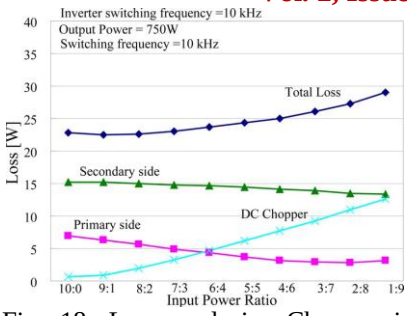

Fig. 18. Loss analysis—Changes in input power ratio (asymmetric method).

For the symmetric method in Fig. 17, it is obvious that the loss in the dc chopper increases sharply as the battery current increases. However, the loss in the primary side does not reach zero, but drops to a constant 4 W from 7 W.

On the other hand, as the generator power is less than 225W, the loss in the secondary side starts to decrease. This is because the output voltage is directly dependent on the input voltage in the IMC. As the input voltage decreases, the magnitude of the output voltage also decreases. However, in the proposed circuit, the boost converter maintains the dc-link voltage, even if the generator power drops; therefore, the output side can maintain its power.

Fig. 18 shows the same analysis with the second condition, where the asymmetric format is applied. As expected, the loss in the primary side remains unchanged; however, the loss in the secondary side is reduced approximately 18% compared to that for the symmetric format in Fig. 17. When the battery is at full power, the loss reduces approximately 25%. This comparison shows that the proposed converter can achieve better efficiency by applying the asymmetric method, and the performance of the boost converter is not limited by the change of carrier.

VII.CONCLUSION

A new control method is proposed by utilizing the neutral point of a motor and connection to an IMC for motor drive applications. Control over the inverter zero-vector periods allows an additional chopper leg to perform as a boost converter with connection to the neutral point of a motor. Simulation and experimental results demonstrated good sinusoidal waveforms and confirmed the validity of the proposed method. From the loss analysis of the proposed circuit, an efficiency of 96% was estimated. EMC behavior of the circuit will be subjected for further investigation.

REFERENCES

[1] D. Casadei, G. Grandi, C. Rossi, A. Trentin, and L. Zarri, "Comparison between back-to-back and matrix converters based on thermal stress of the switches," in *Proc. IEEE Int. Symp. Ind. Electron.*, May 2004, vol. 2, pp. 1081–1086.

[2] R. Ghosh and G. Narayanan, "Control of three-phase, four-wire PWM rectifier," *IEEE Trans. Power Electron.*, vol. 23, no. 1, pp. 96–106, Jan. 2008.

[3] R. Lai, F. Wang, R. Burgos, Y. Pei, D. Boroyevich, B. Wang, T. A. Lipo, V. D. Immanuel, and K. J. Karimi, "A systematic topology evaluation methodology for high-density three-phase PWM AC-AC converters," *IEEE Trans. Power Electron.*, vol. 23, no. 6, pp. 2665–2680, Nov. 2008.

[4] X. H.Wu, S. K. Panda, and J. X. Xu, "Analysis of the instantaneous power flowfor three-phasePWMboost rectifier under unbalanced supply voltage conditions," *IEEE Trans. Power Electron.*, vol. 23, no. 4, pp. 1679–1691, Jul. 2008.

[5] B. Yin, R. Oruganti, S. K. Panda, and A. K. S. Bhat, "A simple singleinput- single-output (SISO) model for a three-phasePWMrectifier," *IEEE Trans. Power Electron.*, vol. 24, no. 3, pp. 620–631, Mar. 2009.

[6] H.Yoo, J.-H.Kim, and S.-K. Sul, "Sensorless operation of aPWMrectifier for a distributed generation," *IEEE Trans. Power Electron.*, vol. 22, no. 3, pp. 1014–1018, May 2007.

[7] Y. Chen and X. Jin, "Modeling and control of three-phase voltage source PWM rectifier," in *Proc. IEEE Power Electron. Motion Control Conf.*, Shanghai, Aug. 2006, vol. 3, pp. 1–4.

[8] R.Vargas, U. Ammann, and J. Rodriguez, "Predictive approach to increase efficiency and reduce switching losses onmatrix converters," *IEEE Trans. Power Electron.*, vol. 24, no. 4, pp. 894–902, Apr. 2009.

[9] M. Jussila and H. Tuusa, "Comparison of simple control strategies of space-vector modulated indirect matrix converter under distorted supply voltage," *IEEE Trans. Power Electron.*, vol. 22, no. 1, pp. 139–148, Jan. 2007.

[10] T. Friedli, M. L. Heldwein, F. Giezendanner, and J. W. Kolar, "A high efficiency indirect matrix converter utilizing RB-IGBTs," in *Proc. 37th IEEE Power Electron. Spec. Conf.*, Jeju, Jun. 2006, pp. 1–7.

[11] J.W. Kolar, F. Schafmeister, S. D. Round, and H. Ertl, "Novel three-phase AC–AC sparse matrix converters," *IEEE Trans. Power Electron.*, vol. 22, no. 5, pp. 1649–1661, Sep. 2007.

[12] J.-I. Itoh and K.-I. Nagayoshi, "A new bidirectional switch with regenerative snubber to realize a simple series connection for matrix converters," *IEEE*

Trans. Power Electron., vol. 24, no. 3, pp. 822–829, Mar. 2009.

[13] T. Wijekoon, C. Klumpner, P. Zanchetta, and P. W. Wheeler, "Implementation of a hybrid AC–AC direct power converter with unity voltage transfer," *IEEE Trans. Power Electron.*, vol. 23, no. 4, pp. 1918–1926, Jul. 2008.

[14] J. Itoh and K. Fujita, "Novel unity power factor circuits using zero-vector control for single-phase input systems," *IEEE Trans. Power Electron.*, vol. 15, no. 1, pp. 36–43, Jan. 2000.

[15] J.-i. Itoh, I. Sato, A. Odaka, H. Ohguchi, H. Kodachi, and N. Eguchi, "A novel approach to practical matrix converter motor drive system with reverse blocking IGBT," *IEEE Trans. Power Electron.*, vol. 20, no. 6, pp. 1356–1363, Nov. 2005.

[16] K. Kato and J.-i. Itoh, "Control method for a three-port interface converter using an indirect matrix converter with an active snubber circuit," in *Proc. 13th Power Electron. Motion Control Conf.*, Poznan, Sep. 2008, pp. 581– 588.

[17] J.-i. Itoh, S. Ikuya, O. Hideki, S. Kazuhisa, O. Akihiro, and E. Naoya, "A control method for the matrix converter based on virtual AC/DC/AC conversion using carrier comparison method," *IEEJ Trans. Ind. Appl.*, vol. 152, no. 3, pp. 65–73, Jun. 2005.

[18] J.-i Itoh, T. Iida, and A. Odaka, "Realization of high efficiency AC link converter system based on AC/AC direct conversion techniques with RBIGBT," in *Proc. 32nd Ann. Conf. IEEE Ind. Electron.*, Paris, Nov. 2006, pp. 1703–1708.

[19] S. Round, F. Schafmeister, M. Heldwein, E. Pereira, L. Serpa, and J. W. Kolar, "Comparison of performance and realization effort of a very sparse matrix converter to a voltage dc link pwm inverter with active front end," *IEEJ Trans. Inst. Electr. Eng. Jpn.*, vol. 126-D, no. 5, pp. 578–588, May 2006.

BIOGRAPHY

Hathiram Guguloth , II-M.Tech P.E, Department of EEE, SV Engineering College, Suryapet.

Santosh A, II-M.Tech P.E, Department of EEE, SV Engineering College, Suryapet.